Title

Probing transference and field-induced polymer velocity in block copolymer electrolytes

Journal

Cell Reports Physical Science, 5(1)

ISSN

2666-3864

Authors

Galluzzo, Michael D

Steinrück, Hans-Georg

Takacs, Christopher J

et al.

Publication Date

2024

DOI

10.1016/j.xcrp.2023.101766

Cell Reports
Physical Science

CellPress
OPEN ACCESS

Article

Probing transference and field-induced polymer velocity in block copolymer electrolytes

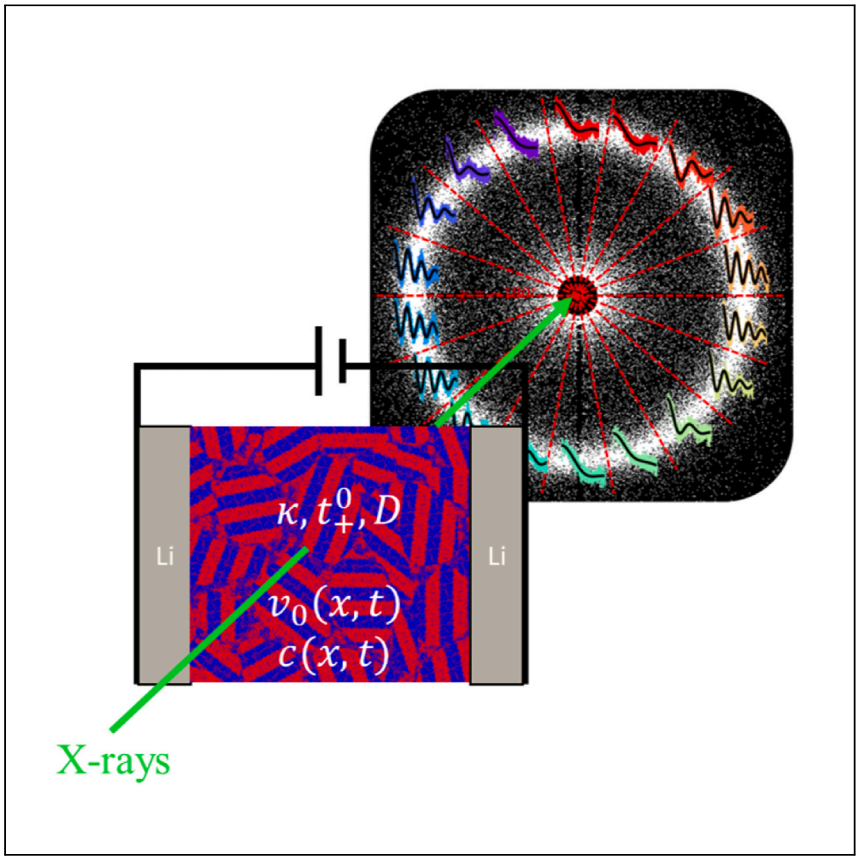

The performance of a battery electrolyte is governed by the velocity and concentration fields that arise during polarization of the cell. Galluzzo et al. investigate the nature of these fields for a block copolymer electrolyte designed for a lithium battery. They find that using a single-solvent approximation to describe the dual-phased electrolyte leads to an inconsistency in the measured transference number under small and large applied electric fields.

Michael D. Galluzzo, Hans-Georg Steinrück, Christopher J. Takacs, ..., Venkat Srinivasan, Michael F. Toney, Nitash P. Balsara

nbalsara@berkeley.edu

Highlights

Experiments and theory provide fundamental insight into battery electrolytes

Direct measurement of velocity and salt concentration fields in a polymer electrolyte

Limitations of the "single-solvent approximation" for block copolymer electrolytes

Investigating the role of the transference number in transport phenomena

Galluzzo et al., Cell Reports Physical Science 5, 101766
January 17, 2024
https://doi.org/10.1016/j.xcrp.2023.101766

Cell Reports
Physical Science

CellPress
OPEN ACCESS

Article

Probing transference and field-induced polymer velocity in block copolymer electrolytes

Michael D. Galluzzo,[1,2] Hans-Georg Steinrück,[3,4,5] Christopher J. Takacs,[6,7] Aashutosh Mistry,[8,9] Lorena S. Grundy,[1,10] Chuntian Cao,[6,11] Suresh Narayanan,[12] Eric M. Dufresne,[12] Qingteng Zhang,[12] Venkat Srinivasan,[8,9] Michael F. Toney,[10,13,14,15] and Nitash P. Balsara[1,2,10,16,*]

SUMMARY

Concentration polarization in an electrolyte comprising dissociated ions and a solvent is often modeled using concentrated solution theory developed by Newman. This theory is built upon two differential equations for electrolyte concentration and solvent velocity fields. We characterize the concentration and solvent velocity fields in a polystyrene-*block*-polyethylene oxide (SEO) block copolymer electrolyte using *operando* X-ray transmission measurements and X-ray photon correlation spectroscopy, respectively. Using calculations based on the assumption that the SEO chain behaves as a single species, we show that the experimental data are consistent with a cation transference number, $t_+^0 \approx 0.7$. Previously published electrochemical experiments using small polarizations led to the conclusion that t_+^0 is less than 0.3. The discrepancy indicates that the block copolymer electrolyte cannot be approximated as a three-component system (cation, anion, and a single solvent), and frictional interactions involving the glassy polystyrene cannot be lumped with those involving rubbery poly(ethylene oxide) segments.

INTRODUCTION

One motivation to study solid polymer electrolytes is to enable electrodes with higher capacity and operating voltages than those that can be used in current lithium-ion batteries. In this paper, we study a polystyrene-*block*-polyethylene oxide (SEO) block copolymer electrolyte where polystyrene (PS) provides mechanical rigidity and polyethylene oxide (PEO) solvates lithium bis(trifluoromethanesulfonyl) imide (LiTFSI) and facilitates ion transport. For binary electrolytes with a single solvent (typically an organic liquid or a homopolymer such as PEO), ion transport is characterized by three independent Stefan-Maxwell diffusion coefficients related to three independent frictional interactions: between the cation and the solvent, between the anion and the solvent, and between the cation and anion.[1] These diffusion coefficients are not measured directly but calculated from a series of electrochemical experiments.[2,3] In concentrated solution theory, the governing mass transport equations can be recast in terms of three measurable transport parameters: ionic conductivity, salt diffusion coefficient, and transference number.

Describing mass transport using three independent parameters is an approximation for systems like SEO/LiTFSI where more than three components are present (Li^+, $TFSI^-$, PS, and PEO). The approximation is equivalent to the assertion that the covalently bonded PS and PEO chains act as a single species. In a rigorous theory, however, one must consider frictional interactions between the ions and both PS and

[1]Department of Chemical and Biomolecular Engineering, University of California, Berkeley, Berkeley, CA 94720, USA

[2]Materials Science Division, Lawrence Berkeley National Laboratory, Berkeley, CA 94720, USA

[3]Department Chemie, Universität Paderborn, 33098 Paderborn, Germany

[4]Forschungszentrum Jülich, Institute for a Sustainable Hydrogen Economy (INW), Am Brainergy Park 4, 52428 Jülich, Germany

[5]RWTH Aachen University, Institute of Physical Chemistry, Landoltweg 2, 52074 Aachen, Germany

[6]SSRL Materials Science Division, SLAC National Accelerator Laboratory, Menlo Park, CA 94025, USA

[7]SLAC National Accelerator Laboratory, Joint Center for Energy Storage Research (JCESR), Menlo Park, CA 94025, USA

[8]Chemical Sciences and Engineering Division, Argonne National Laboratory, Lemont, IL 60439, USA

[9]Joint Center for Energy Storage Research (JCESR), Argonne National Laboratory, Lemont, IL 60439, USA

[10]Joint Center for Energy Storage Research (JCESR), Lawrence Berkeley National Laboratory, Berkeley, CA 94720, USA

[11]Computational Science Initiative, Brookhaven National Laboratory, Upton, NY 11973, USA

[12]Advanced Photon Source, Argonne National Laboratory, Lemont, IL 60439, USA

[13]Department of Chemical and Biological Engineering, University of Colorado Boulder, Boulder, CO 80303, USA

[14]Department of Materials Science and Engineering, University of Colorado Boulder, Boulder, CO 80303, USA

[15]Renewable and Sustainable Energy Institute, University of Colorado Boulder, Boulder, CO 80303, USA

[16]Lead contact

*Correspondence: nbalsara@berkeley.edu

https://doi.org/10.1016/j.xcrp.2023.101766

PEO as well as those between PS and PEO, totaling six independent parameters. In addition, the volume fraction of the ion conduction domain is thermodynamically linked to the polarization of the electrolyte through the salt concentration gradient.[4,5] The stress induced by the salt concentration gradient and volume changes of the conduction phase must also be considered.[6–9] While developments in theory and experiment have begun to address these effects,[10–20] a rigorous framework for complete electrochemical characterization (i.e., measurement of a set of transport and thermodynamic parameters which allows for the calculation of concentration, velocity, and potential fields with no adjustable parameters) has not yet been developed. Within the field of block copolymer electrolytes, it is thus common to interpret electrochemical data using the framework developed for a binary electrolyte with a single solvent species; we refer to this assumption as the "single-solvent approximation." Despite obvious limitations, this approach has provided fundamental insight into the nature of ion transport.[21–28] In this work, we examine these limitations using direct measurements of the velocity and concentration fields in a polarized block copolymer electrolyte.

In an electrolyte, an externally applied electric field results in motion of the charged species. The velocities of the species are governed by the frictional interactions introduced above. Frictional interactions between the ions and the solvent also result in a net velocity of the neutral solvent. Direct measurement of species velocities is challenging but important because it provides insight into the frictional interactions within the electrolyte (i.e., the Stefan-Maxwell diffusion coefficients). For example, the net velocity of a cation in an electric field will be directly related to the frictional "drag" imposed by the solvent and the anion. Direct measurements of species velocities thus provide insight into ion transport that is difficult to glean from electrochemical characterization alone.[29]

The current density through an arbitrary reference volume is proportional to the flux of ions, which is, in turn, proportional to the velocity of the ions. Two approaches for measuring species velocities have been established: electrophoretic nuclear magnetic resonance (eNMR)[30,31] and X-ray photon correlation spectroscopy (XPCS).[32] eNMR can measure the field-induced velocities of any species that contain an NMR-active atom, but it has, thus far, only been used to measure the initial velocities of the species. By definition, these velocities are independent of spatial coordinates in the cell. In contrast, XPCS has been used to measure the solvent velocity only, but with spatial and temporal resolution. The technique was established using a PEO/LiTFSI electrolyte.[32] In this work, we apply the same technique to an SEO/LiTFSI electrolyte. In addition to XPCS, we use time and spatially resolved measurements of X-ray transmission to determine the evolution of salt concentration gradient.[33] Both X-ray measurements were made in *operando* lithium symmetric cells.

Here we show that the transference number required to explain the experimental data utilizing the single-solvent approximation is significantly larger than that inferred from electrochemical experiments. We obtain a value of $t_+^0 \approx 0.7$, whereas values less than 0.3 have been reported for SEO/LiTFSI electrolytes.[2,34] In the case of PEO/LiTFSI, there was no significant discrepancy between the measured PEO velocity and transference numbers determined by electrochemical methods.[32] Our result indicates a failure of the single-solvent approximation, which embeds the assumption that the frictional interactions between an ion (either anion or cation) and the solvent can be quantified by a single Stefan-Maxwell diffusion coefficient. We hypothesize that in a block copolymer electrolyte such as SEO, the frictional interactions between the ions and the individual PS and PEO blocks must be accounted

for separately. This is due to the glassy nature of the PS microphase and the rubbery nature of the PEO microphase. In addition, concentrated solution theory assumes that the stress stored in the electrolyte is negligible, even in the presence of current. This may not be true when the electrolyte contains glassy microphases.

RESULTS AND DISCUSSION

XPCS experiments

The electrolyte used in our study was an SEO/LiTFSI electrolyte with PS and PEO molecular weight of 19 and 20 kg mol^{-1}, respectively, and molar ratio of LiTFSI to ethylene oxide units, r, of 0.08. Our work follows the methods laid out by Steinrück et al. where electrolyte velocity is measured via *operando* heterodyne XPCS.[32] An electrochemical cell was devised with lithium electrodes sandwiched around a block copolymer electrolyte, and the sample temperature was maintained at 90°C using a copper heating block. The sample was hermetically sealed, and the chamber was flushed with helium to avoid moisture contamination. XPCS experiments were conducted at beamline 8-ID-I at the Advanced Photon Source. The X-ray beam is passed through the electrolyte, parallel to the electrodes. The size of the beam (15 × 15 μm) was much smaller than the distance between electrodes (3 mm), such that we can assume the electrolyte properties as constant within the sampled region. A second compartment was included in the sample holder and filled with the same electrolyte but was not attached to any electrodes and used as a heterodyne reference.[35] The beam passed first through the electrochemical channel followed by the reference. The path length of the beam through the reference electrolyte channel and the electrochemical channel were both equal to 1 mm. A schematic of the experimental setup is shown in Figure 1A and a picture is shown in Figure S1.

In a typical heterodyne XPCS experiment,[36–38] coherent scattering patterns are collected at regular intervals for some duration of time (in our case every 60 ms for 360 s). The scattering pattern is a mix of the scattering from the dynamic sample (where the scatterers are assumed to have some net velocity) and a static reference sample (where the scatterers are assumed to have no net velocity). The ratio of scattering intensity from the dynamic sample relative to the sum of the dynamic and reference sample is the heterodyne fraction, h. Because the path lengths through the dynamic and reference sample were equal, we take $h = 0.5$. The velocity of the scatterers in the dynamic sample (assumed to be constant over the course of a 360-s data acquisition window) compared to the stagnant reference yields a phase shift in the coherent scattering. This is captured as oscillations in the autocorrelation function, $g_2(\boldsymbol{q},\tau)$, which correlates the intensity of scattering at a given scattering vector, $\boldsymbol{q}$, at time t and that at time $t+\tau$ where τ is the time delay. The autocorrelation function is given by[39]:

$$g_2(\boldsymbol{q},\tau) = 1 + \beta(1-h)^2 + h^2\beta \exp\left[-2\left(\frac{\tau}{\tau_0(\boldsymbol{q})}\right)^{\gamma}\right] + 2h(1-h)\beta\cos(\omega\tau)\exp\left(\frac{\tau}{\tau_0(\boldsymbol{q})}\right)^{\gamma}, \quad \text{(Equation 1)}$$

where

$$\omega = \boldsymbol{q}\cdot\boldsymbol{v} = qv\left|\cos\chi\right| \quad \text{(Equation 2)}$$

In Equation 1, χ is angle between $\boldsymbol{q}$ and the velocity of the scatterers, $\boldsymbol{v}$, β is the coherence factor, and τ_0 is the relaxation time of the sample. The right side of Equation 2 contains a $|\cos\chi|$ term because XPCS is only sensitive to the magnitude of $\boldsymbol{v}$

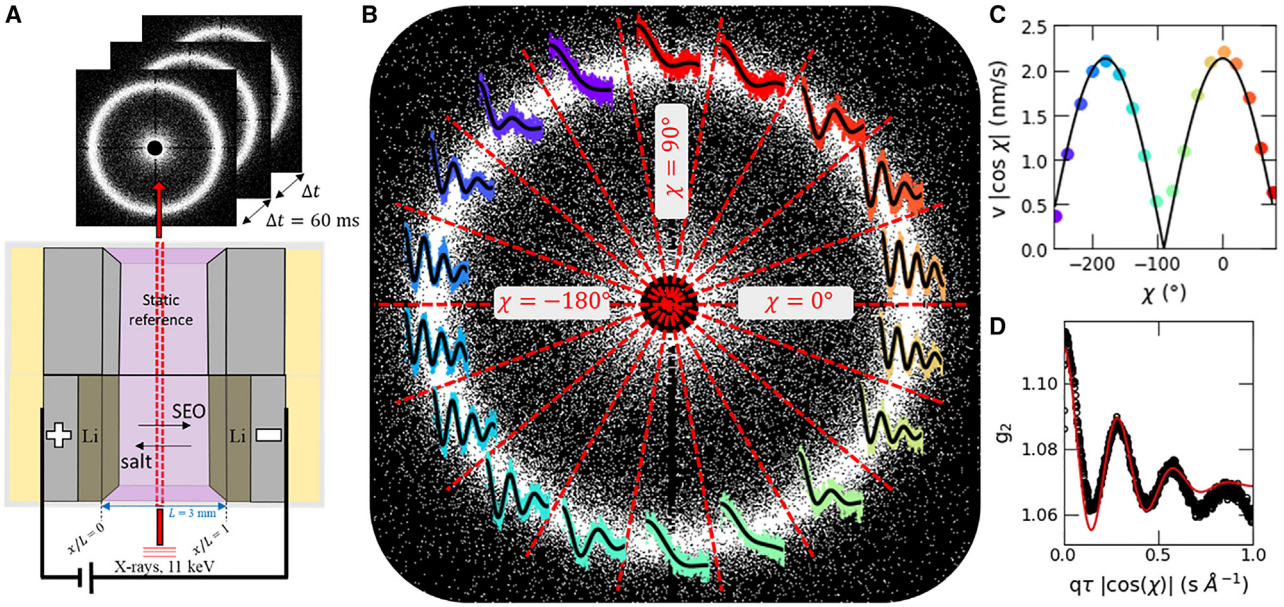

Figure 1. XPCS experimental setup, autocorrelation functions, and fits to the data

(A) Schematic of the experimental setup. X-rays pass through the dynamic block copolymer electrolyte sample, which is sandwiched by lithium metal electrodes and attached to a potentiostat followed by the static reference sample. The distance between electrodes, L, is 3 mm where the normalized x coordinate, x/L, is defined to be 0 at the left electrode and 1 at the right electrode. Coherent scattering patterns are obtained every 60 ms for 360 s (6,000 patterns per measurement).

(B) Representative SAXS pattern for one measurement obtained at t = 1.4 h during a 200-mV mm^{-1} polarization. Red dashed lined indicates the χ bins used for collapsing the autocorrelation functions. The colored curves in each dataset represent the autocorrelation function, g_2, collapsed along the q axis. Black lines are fits to the data based on Equation 1.

(C) Velocity, $v|cos\ \chi|$, measured as a function of χ for the curves in (B). The black line is a fit to Equation 2.

(D) Result of collapsing the autocorrelation functions along all χ values (black data points). The red line is the fit to the experimental data from Equation 1, yielding a measured velocity of 2.13 nm s^{-1}.

(not direction). A stretched exponential decay with stretching factor γ is used to model the sample relaxation. Equations 1 and 2 allow us to collapse all correlation functions along q and τ as described by Steinrück et al.[32]

In a microphase-separated block copolymer, fluctuations arise due to differences in electron density (contrast) between the two microphases.[40,41] In SEO/LiTFSI electrolytes, salt resides primarily in the PEO-rich domains and is excluded from the PS-rich domains.[42] The X-ray scattering profiles reflect the inhomogeneous distribution of electron density in the sample. Because the range of scattering angles measured was chosen to coincide with the domain size of the PS-PEO lamellae (we will discuss this shortly), and the scattering arises primarily due to the contrast between the PS-rich and PEO/salt-rich domains, our experiment probes the velocity of the PS-PEO lamellae (polymeric "solvent") in response to the applied electric field. For simplicity, we refer to the velocity measured by XPCS as the polymer (or solvent) velocity.

In Figure 1, we present the XPCS results upon imposition of a constant electric field of 200 mV mm^{-1}; t = 0 h = 0 h is defined as the moment that the potential was initiated across the cell by the potentiostat. A single XPCS experiment yields 6,000 small-angle X-ray scattering (SAXS) patterns that are used to calculate the autocorrelation function, g_2. In Figure 1B, we present the 2D SAXS profile from our sample averaging over all 3,600 scans. The q-range sampled in our experiment is $0.029 < q < 0.28$ nm^{-1} where q is the magnitude of the scattering vector, $\boldsymbol{q}$. The

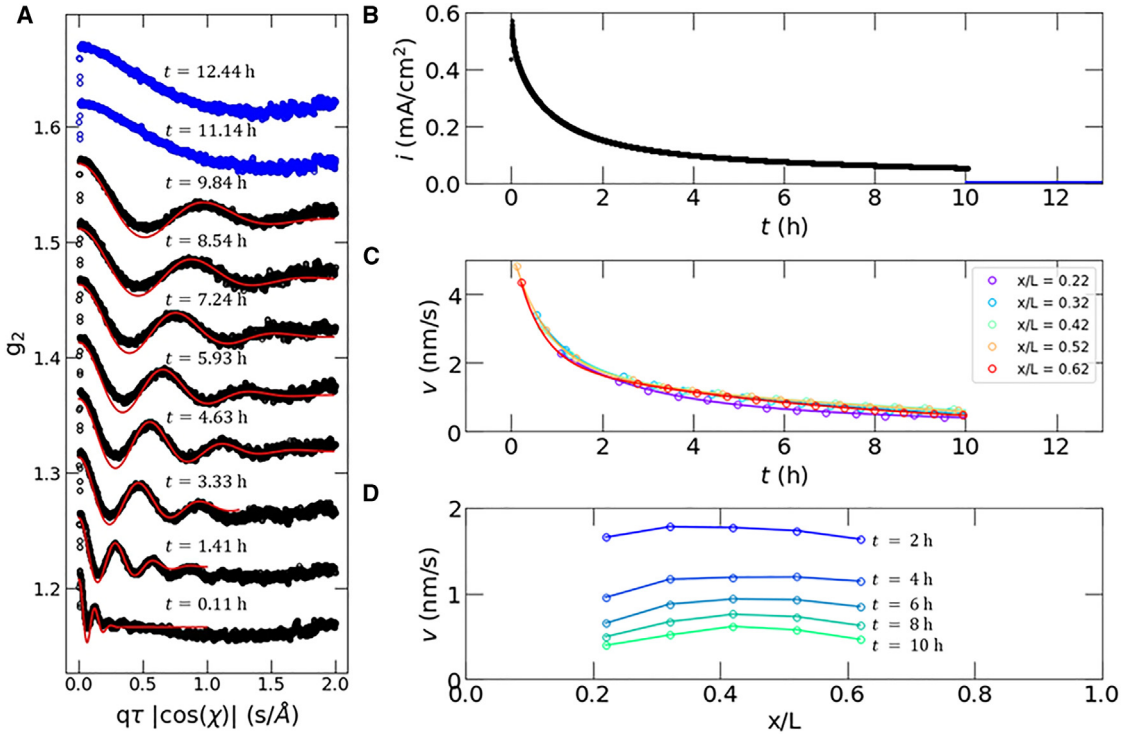

Figure 2. Polarization-induced polymer velocity as a function of time and position from XPCS autocorrelation functions

(A) Autocorrelation functions, g_2, obtained from an SEO/LiTFSI electrolyte polarized at 200 mV mm^{-1} (black datasets) as a function of time (offset for clarity) at a position in the cell corresponding to $x/L = 0.52$. Red lines are fits to the data used to obtain the velocity at each time point. Blue datasets were obtained after switching the current to zero.

(B) Current density measured during the polarization experiment (black data points). The blue data points at t > 10 h indicate the cell was switched to open circuit.

(C) Velocity as a function of time for five positions in the cell. The solid lines are polynomial fits to the data used to extrapolate to between the points.

(D) Velocity as a function of position in the cell at t = 2, 4, 6, 8, and 10 h.

2D profile contains a bright ring of intensity corresponding to the primary scattering peak, q^*, of the SEO lamella at $q = 0.16$ nm^{-1} and a lamellar spacing, d, of 39.3 nm ($d = 2\pi/q^*$). Based on Equation 1, the frequency of oscillation in the autocorrelation function, ω, is maximized when $\cos\chi = 1$, i.e., $\chi = 0$ or $= 180°$. We define $\chi = 0°$ as the angle along the positive x axis in Figure 2A. We divide the spectra into 18 azimuthal slices along which we binned the data. In Figure 1C, we plot g_2 versus $q\tau$ averaged for all values of q within each bin. The data are reproduced with the axis labels in Figure S2. The black lines in Figure 1B show the fits to the data based on Equation 1, which we use to obtain the magnitude of ω. Since q is known, $v|\cos\chi|$ can be calculated from the fit at each value of χ. The results are shown in Figure 1C. As expected, $v|\cos\chi|$ is maximized for $\chi = 0°$ and $\chi = -180°$, and it approaches zero at $\chi = 90°$ and $\chi = -270°$. The black curve in Figure 1C is a plot of $v|\cos\chi|$ with the value of v adjusted to match the maxima in the measurements. These data prove that the polymer velocity is either in the direction $\chi = 0°$ or $\chi = -180°$. Based on concentrated solution theory,[1] we anticipate the direction of the polymer velocity will be down the salt concentration gradient, i.e., along $\chi = 0°$ (from left to right in Figure 1A). To calculate the magnitude of the velocity, we collapse the data from a single experiment along all bins by plotting g_2 as a function of $q\tau\cos\chi$. An example is shown in Figure 1D. We then fit the data (solid red line in Figure 1D) using Equation 1 to obtain the velocity (2.13 nm s^{-1} in the example). We performed these experiments at five positions in the cell and

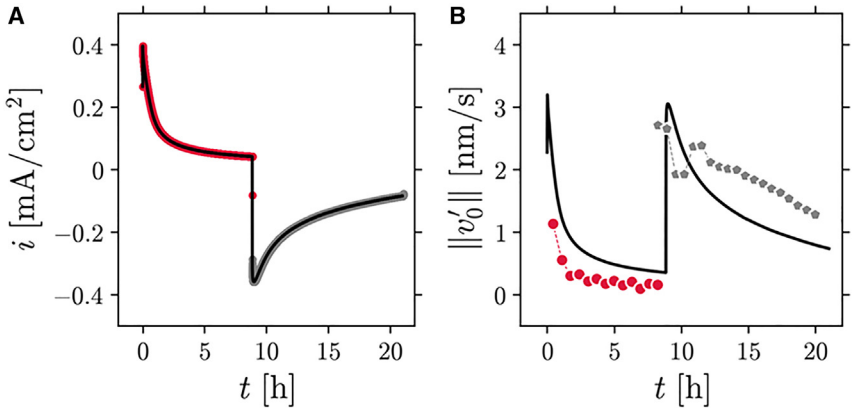

Figure 3. Comparison of XPCS-measured polymer velocity and theoretical calculations

(A) Current density measured in the XPCS cell in response to a +200 mV mm^{-1} polarization from t = 0 to 9 h (red data points) followed by immediately switching the polarization to −200 mV mm^{-1} from t = 9 to 21 h (gray data points). The black line is a fit to the data.

(B) XPCS velocity measurements obtained at x/L = 0.52 as a function of time. Red data points correspond to the +200 mV mm^{-1} polarization, and gray data points correspond to the −200 mV mm^{-1} polarization. The black line corresponds to the theoretical calculations with $t_+^0 = 0.7$ and $D = 10^{-8}$ cm^2 s^{-1}.

repeated them at selected times to obtain velocity measurements as a function of time and position along the horizontal axis, x/L.

In Figure 2, we summarize the XPCS data obtained after the application of a field of 200 mV mm^{-1}. The autocorrelation function collapsed in q and χ is plotted in Figure 2A at selected time points for the dataset obtained at $x/L = 0.52$, offset vertically for clarity. The electric field was applied for 10 h. The current density, i, measured by the potentiostat while the potential was applied is plotted in black data points in Figure 2B. The blue line at $i = 0$ mA cm^{-2} beginning at $t = 10$ h indicates the time at which the cell was switched to open circuit. The black datasets in Figure 2A correspond to measurements taken while the cell was under polarization, and the blue datasets (for $t > 10$ h) were obtained while the cell was under the open circuit condition. Red lines in Figure 2A are fits of Equation 1 through the data. The frequency of oscillation in the g_2 functions decreases from $t = 0.11$ h to $t = 9.84$ h, which indicates a decrease in solvent velocity. When the current is set to zero (blue datasets at $t = 11.14$ *and* 12.44 h), no oscillations in the g_2 function are observed, indicating that the polymer velocity is approximately zero. The velocity during the polarization step, obtained by fitting the curves in Figures 2A, is plotted in Figure 2C as a function of time for five positions in the cell: $x/L = 0.22$, 0.32, 0.42, 0.52, and 0.62. As soon as the field is applied ($t = 0$), the polymer velocity is approximately 4.5 nm s^{-1}. The velocity decays to 0.65 nm s^{-1} at $t = 10$ h. This indicates that the system did not achieve steady state in the 10-h polarization experiment because the polymer velocity will approach zero at steady state. The solid curves in Figure 2C are polynomial fits to the data that were used to interpolate between data points and to obtain $v(x/L)$ at fixed t. We plot v vs. x/L at $t = 2$, 4, 6, 8, and 10 h in Figure 2D. At all times, the velocity is maximized near the center of the cell ($x/L = 0.5$).

In the next experiment, XPCS data were acquired using a fresh sample while a field of +200 mV mm^{-1} was applied for 9 h and then immediately flipped to −200 mV mm^{-1}. The current response of the cell is shown in Figure 3A as red data points for the +200 mV mm^{-1} polarization and gray data points for the −200 mV mm^{-1} polarization. The black line in Figure 3A is a fit to the data used to interpolate $i(t)$ for the

theoretical calculations. In Figure 3B, the red and gray data points represent the velocity measurements obtained at $x/L = 0.52$, near the middle of the cell. We plot the absolute value of the velocity on the y axis because our XPCS cannot differentiate between velocity directed in the +x or –x direction. We mentioned above that we expect the polymer velocity in the first polarization step to be in the +x direction. Using analogous arguments, we expect the polymer velocity in the second polarization step to be in the –x direction. During the first 9 h, we obtain the expected monotonic decay in velocity from 1.2 nm s^{-1} to 0 nm s^{-1} (red data points). We notice a significant difference in the magnitude of the initial velocity in Figure 2C at $t = 0$ h (4.5 nm s^{-1}) and Figure 3B at $t = 0$ h (1.2 nm s^{-1}), even though the magnitude of the polarization was the same. This is related to differences in the interfacial resistance in the two samples (see Figure S3 and discussion in the supplemental information). When the potential is flipped to −200 mV mm^{-1}, the magnitude of the velocity increases compared to the first polarization (gray data points). Interestingly, the velocity change is nonmonotonic: the polymer velocity decreases rapidly between 9 and 10 h and increases between 10 and 11 h before decaying for longer times. While we only show one position in the cell in Figure 3B, we observed this nonmonotonic behavior in all five positions that were measured in the cell (see Figure S4).

Theoretical interpretation

We use concentrated solution theory with the single-solvent approximation to interpret the XPCS data. In this theory,[1,43] the governing equations for salt concentration, c, and polymer (solvent) velocity, v_0, are as follows:

$$\frac{\partial c}{\partial t} = \frac{\partial}{\partial x}\left(D\left(1 - \frac{\mathrm{d}\ln c_0}{\mathrm{d}\ln c}\right)\frac{\partial c}{\partial x} - t_+^0\frac{i}{F} - cv_0\right), \qquad \text{(Equation 3)}$$

$$\frac{\partial v_0}{\partial x} = \overline{V}\frac{\partial}{\partial x}\left(D\left(1 - \frac{\mathrm{d}\ln c_0}{\mathrm{d}\ln c}\right)\frac{\partial c}{\partial x} - t_+^0\frac{i}{F}\right) \quad . \qquad \text{(Equation 4)}$$

Here c is the moles of LiTFSI per unit electrolyte volume, which contains PEO and PS chains. In the same spirit, v_0 refers to the continuum velocity of PEO and PS chains in the lamellar domains. Since the PEO and PS are covalently bonded, they move at identical velocities. $\overline{V}$ is the partial molar volume of the salt, D is the salt diffusion coefficient, and t_+^0 is the cation transference number with respect to the solvent velocity. x represents a moving coordinate system (with respect to the lab reference frame) with $x = 0 = 0$ attached to the Li electrode on the left side in Figure 1A. This nuance is because the Li/electrolyte interface moves with respect to the laboratory as lithium is plated at the negative electrode and stripped at the positive electrode. Appropriate boundary conditions to solve Equations 3 and 4 are shown:

$$x = 0 \text{ boundary}: \quad -D\left(1 - \frac{\mathrm{d}\ln c_0}{\mathrm{d}\ln c}\right)\frac{\partial c}{\partial x} = \left(1 - t_+^0\right)\frac{i}{F}, \qquad \text{(Equation 5)}$$

$$v_0 = 0, \qquad \text{(Equation 6)}$$

$$x = L \text{ boundary}: \quad -D\left(1 - \frac{\mathrm{d}\ln c_0}{\mathrm{d}\ln c}\right)\frac{\partial c}{\partial x} = \left(1 - t_+^0\right)\frac{i}{F}. \qquad \text{(Equation 7)}$$

Four properties appear in these equations: D, $\left(1 - \frac{\mathrm{d}\ln c_0}{\mathrm{d}\ln c}\right)$, t_+^0, and $\overline{V}$. D and t_+^0 are transport properties. $\left(1 - \frac{\mathrm{d}\ln c_0}{\mathrm{d}\ln c}\right)$ and $\overline{V}$ are thermodynamic properties related to electrolyte density, ρ. ρ can be expressed for LiTFSI/PEO/PS mixtures using LiTFSI/PEO density data, PS density, and number averaged molecular masses of PEO and PS, assuming that all of the LiTFSI resides in the PEO-rich lamellae. Appropriate fitting relations based on Figure S5 are as follows:

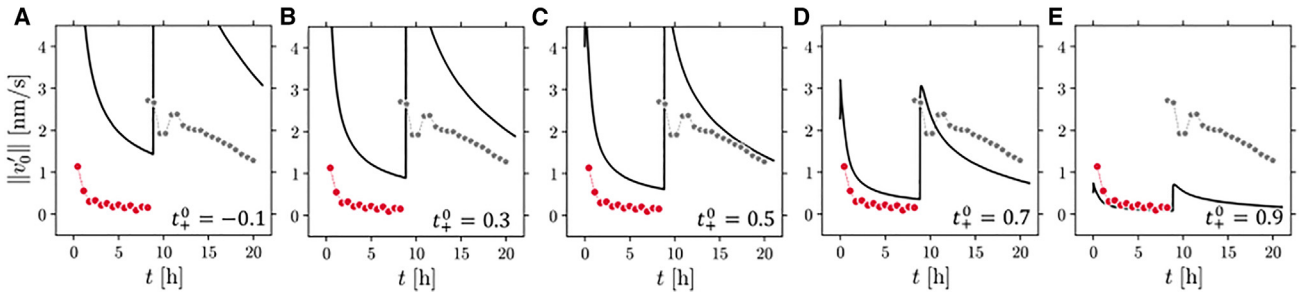

Figure 4. Comparison of predicted v_0 based on different values of t_+^0 to XPCS-measured polymer velocity

(A) $t_+^0 = -0.1$.
(B) $t_+^0 = 0.3$.
(C) $t_+^0 = 0.5$.
(D) $t_+^0 = 0.7$.
(E) $t_+^0 = 0.9$.

$$\rho = 0.65 + 0.071c + 0.0056c^2, \quad \text{(Equation 8)}$$

$$r = c(0.060 + 0.027c), \quad \text{(Equation 9)}$$

$$\varepsilon_c = 0.49 + 0.080c - 0.0044c^2 \quad . \quad \text{(Equation 10)}$$

Here, ρ is expressed in g cm^{-3}, c is moles of LiTFSI per liter of electrolyte, r is the ratio of Li^+ cations to ethylene oxide monomer, and ε_c is the volume fraction of LiTFSI/PEO domains, i.e., $(1 - \varepsilon_c)$ is the volume fraction of the PS domains. Equation 8 provides $\left(1 - \frac{\mathrm{d}\ln c_0}{\mathrm{d}\ln c}\right)$ and $\overline{V}$ as a function of salt concentration, c, as shown in Figure S5. Equations 9 and 10 can be used to obtain r and ε_c fields by analyzing the concentration field obtained by solving Equations 3 and 4. The two remaining parameters are t_+^0 and D. In both PEO/LiTFSI and SEO/LiTFSI, D is a weak function of c.[34,44,45] This may seem surprising at first, as frictional interactions increase with increasing salt concentration, and one may thus expect D to decrease with increasing c. However, the salt activity coefficient in these electrolytes increases rapidly with c. The two effects are nearly balanced in PEO-based electrolytes, and the result is that D is nearly independent of c. Based on extensive characterization,[34] we expect $D = 10^{-8}$ cm^2 s^{-1} for a compositionally symmetric SEO electrolyte with total molecular weight of 39 kg mol^{-1}. The value of t_+^0 used in our calculations was 0.7; the reason for this choice will be clarified shortly. Solving Equations 3 and 4 enable determination of c and v_0 as a function of t and x when $i(t)$ is known. Since the experimentally measured v_0 is based on the laboratory reference frame, the velocity of the electrode was subtracted from the calculated v_0 to compare velocities in the same reference frame. We denote the magnitude of the polymer velocity corrected for the velocity of the electrode as $\|v_0'\|$. The calculated value of $\|v_0'\|$ during the two polarization steps is represented by the solid curves in Figure 3B based on the $i(t)$ data from Figure 3A. We could not obtain perfect agreement between the experimental and theoretical calculations, which we attribute to simplifications to the theory: the single-solvent approximation and taking transport parameters to be independent of concentration. Compared to other choices for t_+^0 (see Figure 4), our calculations are in reasonable agreement with the experimental measurements, except for the nonmonotonic dependence of $\|v_0'\|$ soon after the polarization is switched.

In our approach, we fix D for reasons discussed above, and t_+^0 is the only adjustable parameter. In Figure 4, we compare experimentally determined $\|v_0'\|$ with theoretical predictions for a range of t_+^0 values from −0.1 to 0.9. It is obvious that

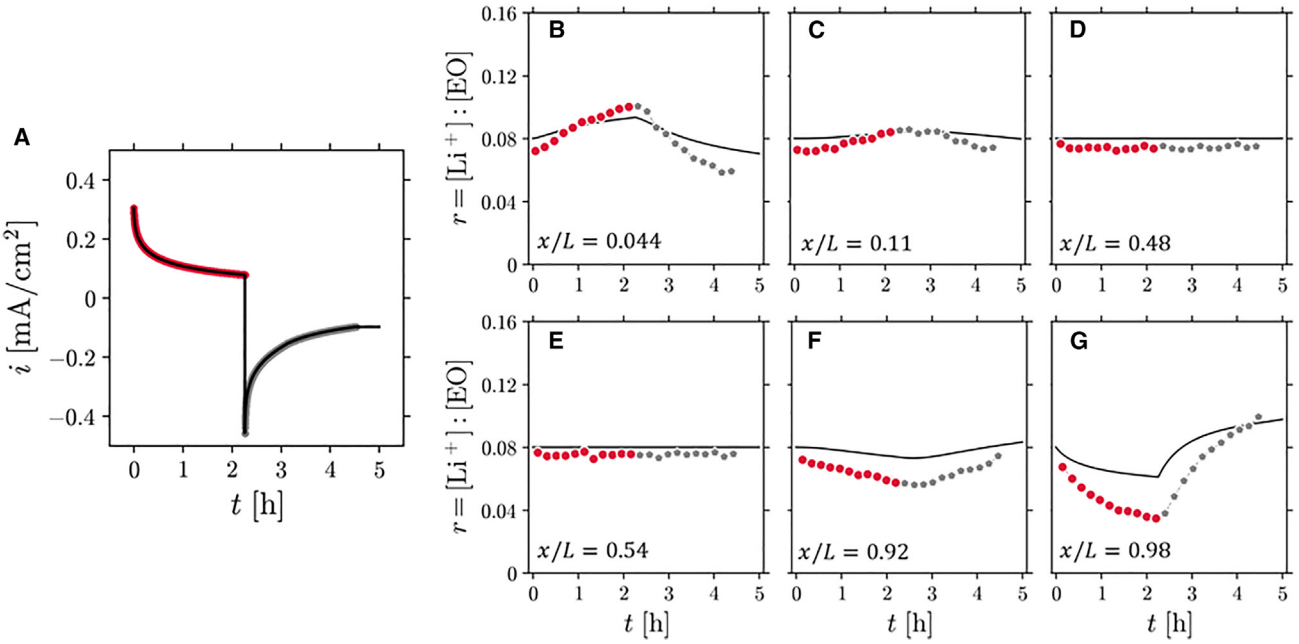

Figure 5. Salt concentration as a function of time and position in a polarized cell measured experimentally by X-ray transmission and compared to theoretical calculations

(A) Current density measured in the SAXS cell in response to a +200 mV mm^{-1} polarization from t = 0 to 9 h (red data points) followed by immediately switching the polarization to −200 mV mm^{-1} from t = 9 to 21 h (gray data points).

(B–G) Local salt concentration, *r*, measured as a function of time in response to the +200 mV mm^{-1} (red datasets) and then −200 mV mm^{-1} (gray datasets) polarization. The black lines correspond to the theoretical calculations with $t_+^0 = 0.7$ and $D = 10^{-8}$ cm^2 s^{-1}.

measurements of $\|v_0'\|$ during the two-step polarization enable discriminating between different values of t_+^0. When t_+^0 is less than 0.7, the calculations overestimate the polymer velocity during both steps. When the t_+^0 is set to 0.9, the polymer velocity during the first step is accurately captured, but the second step velocity is severely underestimated. t_+^0 values in the vicinity of 0.7 capture the measured polymer velocity at the center of the cell during both polarization steps.

The XPCS experiments provide 2D SAXS patterns and X-ray transmission data that can be directly interpreted to probe the structure of the block copolymer and local salt concentration. However, the data are convoluted because the beam passes through two samples: the electrochemically active sample and the static reference. We were thus motivated to perform additional X-ray experiments on a sample without the static reference sample. The cell geometry for these experiments has been described in previous work[6,9] with a distance between electrodes, *L*, of 0.16 cm. To study the same electrochemical conditions, we scaled the potential applied by *L* and time of polarization in each direction by L^2. A detailed study on the correlation between block copolymer morphology and salt concentration gradient on this block copolymer electrolyte system has been presented previously.[7] Here, we focus on the salt concentration as a function of time and position obtained from the X-ray transmission data and comparison to theoretical predictions. The methods for determining the salt concentration from X-ray transmission are presented in the supplemental information and Grundy et al.[6]

The current response in the cell is plotted in Figure 5A as red and gray data points for the positive and negative polarization, respectively. The black line is a fit to the

data to be used in Equations 3, 4, 5, 6, and 7. In Figures 5B–5G, we present the salt concentration, r, as a function of time for x/L = 0.044, 0.11, 0.48, 0.54, 0.92, and 0.98, respectively, where red data points indicate the +200 mV mm^{-1} polarization, and gray data points indicate the −200 mV mm^{-1} polarization. Near the positive electrode (x/L = 0.044), the salt concentration increases rapidly in response to the +200 mV mm^{-1} polarization and then decreases rapidly when the potential is flipped to −200 mV mm^{-1}. The opposite is true near the negative electrode (x/L = 0.98). Near the center of the cell (x/L = 0.48 and 0.54), the salt concentration is approximately constant with time. For all positions in the cell, the salt concentration as a function of time is monotonic once the cell polarization is flipped to −200 mV mm^{-1}. There is no indication of nonmonotonic behavior in either the experimental or theoretical data that would explain the nonmonotonic behavior in the XPCS results.

Theoretical predictions for the salt concentration as a function of time and position were calculated using Equations 3, 4, 5, 6, 7, 8, 9, and 10 and t_+^0 = 0.7 and D = 10^{-8} cm^2 s^{-1}. The fits to the data are shown with black curves in Figures 5B–5G, and reasonable agreement is seen between theory and experiment. The predictions for different values of t_+^0 are shown in Figure S6. We observe reasonable agreement between the experimental values of r and the theoretical predictions when values of t_+^0 of 0.5 and 0.7 are used and poor agreement when values of 0.3 or 0.9 are used. However, using t_+^0 = 0.5 overestimates the value of v_0 by a factor of four and two when the polarization is turned on and flipped in direction, respectively (see Figure 4C). Therefore, the $v_0(x,t)$ and $r(x,t)$ data are best interpreted using $t_+^0 \approx 0.7$ when taking into account the experimentally measured solvent velocity field (via XPCS) and salt concentration field (via X-ray transmission).

Our method of fitting the experimental $v_0(x,t)$ and $r(x,t)$ data yields a much higher transference number compared to what has been previously measured for SEO/LiTFSI electrolytes.[34] The values of t_+^0 for SEO/LiTFSI electrolytes with volumetrically symmetric PS and PEO domains and r between 0.05 and 0.1 obtained by traditional electrochemical methods range between −2 and +0.3.[2,34] The methodology for obtaining t_+^0, which has been established in the literature,[44–46] relies on experiments where small polarizations (typically <10 mV mm^{-1}) are applied to a lithium symmetric cell. When large polarizations are used, we obtain significantly smaller polymer velocities than those anticipated from an electrolyte with $t_+^0 < 0.3$; see Figures 4A and 4B. We postulate that this is due to the stress induced by the changes in conducting phase volume fraction and slow dynamics associated with block copolymer chains rearranging to accommodate the salt concentration gradient. In other words, the impact of the interactions between the PS and other components is more clearly observed when the applied electric field is large. We have previously demonstrated, using the same SEO copolymer, that concentrated solution theory calculations based on the assumption of a three-component system can accurately predict the formation of salt concentration gradients when the current density is less than ~20% of the limiting current but fails as the current density approaches the limiting current.[7]

If we were able to measure the velocities of all three species in our electrolyte at t = 0, then t_+^0 for a single-solvent electrolyte is given by

$$t_+^0 = \frac{v_+ - v_0}{v_+ - v_-}, \qquad \text{(Equation 11)}$$

where v_+ and v_- are the average velocities of cation and anion, respectively. It is evident from Figure 4B that the measured value of v_0 at t = 0 is much lower than

that expected from an electrolyte with $t_+^0 = 0.3$ (a generally accepted value for PEO-containing electrolytes). We posit that the larger-than-expected transference number is related to the slower than expected movement of the polymer chains in response to the relatively large ionic currents in the XPCS experiment. In other words, the ability of the solvent (in this case, the block copolymer) to rearrange to accommodate the salt concentration gradient has a direct impact on the transport of the working cation between the electrodes. This effect will be directly related to the properties of the block copolymer electrolyte. Based on our analysis, we expect a greater enhancement of the transference number if the volume fraction of PS increases as more work would be required to induce flow of the PS domains by the expanding and contracting PEO domains. A smaller enhancement would be observed for electrolytes with lower salt concentrations because the magnitude of the salt concentration gradient would be smaller.

Application of concentrated solution theory allows transport and thermodynamic properties measured at equilibrium or under very small perturbations away from equilibrium to be used to quantify ion transport under arbitrarily large ionic currents. In this work, we show that $t_+^0 = 0.7$ is needed to interpret the XPCS and X-ray transmission measurements, while values less than 0.3 are obtained in electrochemical experiments wherein very small currents are used. This discrepancy indicates a failure in the assumption that an SEO/LiTFSI electrolyte behaves as a three-component system. A quantitative explanation must start with the derivation of appropriate governing equations for solvents with two covalently linked species, which must replace Equations 3 and 4. This framework will contain six transport coefficients. While t_+^0, as defined by Equation 11, is one of them, the other parameters need to be defined and measured. In addition, it will be important to measure ion velocities explicitly to obtain t_+^0. Such a framework may shed light on the nonmonotonic trend in v_0 observed after switching the direction of polarization. The value of t_+^0 presented here is as an approximate transport coefficient that may be used if the solvent is approximated to comprise only one species.

In summary, concentrated solution theory is built upon two differential equations for concentration and solvent velocity fields. A combination of XPCS and X-ray transmission enable direct measurement of these two fields. Our measurements reveal that for block copolymer electrolytes with a glassy block (polystyrene), conventional measurements of transference using electrochemical methods and small applied potentials are inconsistent with the fields obtained under large applied potentials. The measurements show that cation transference under large applied potentials is enhanced due to frictional interactions and strain effects involving the glassy block. These effects are not captured by measurements of t_+^0 using concentrated solution theory with the single-solvent approximation. A generalized framework for characterizing ion transport to account for these interactions remains an unmet challenge.

EXPERIMENTAL PROCEDURES

Resource availability

Lead contact

Requests for further information, resources, or materials should be directed to and will be fulfilled by the lead contact, Nitash Balsara (nbalsara@berkeley.edu), upon reasonable request.

Materials availability

This study did not generate new unique materials.

Data and code availability

The data associated with this work are presented throughout the main text and supplemental information. Raw electrochemical data and parameters obtained from fitting the g_2 autocorrelation functions in this manuscript can be accessed at https://doi.org/10.5281/zenodo.10251535. The depository includes an additional dataset that demonstrates that the second "hump" in velocity (see Figures 3 and S5) that is observed after switching the direction of polarization was replicated in a separate experiment. The raw XPCS and X-ray transmission data will be supplied by the lead contact, Nitash Balsara (nbalsara@berkeley.edu), upon reasonable request. This paper does not report original code. A checklist verifying the integrity of the theoretical predications based on Mistry et al.[47] is included as Table S1 in the supplemental information.

Methods

The experimental methods for the preparation of the electrolyte, preparation of the electrochemical cells, details of the XPCS experiments for measuring velocity fields, and details of the X-ray transmission for measuring concentration fields are provided in the supplemental information section titled "supplemental experimental procedures."

SUPPLEMENTAL INFORMATION

Supplemental information can be found online at https://doi.org/10.1016/j.xcrp.2023.101766.

ACKNOWLEDGMENTS

This work was supported as part of the Joint Center for Energy Storage Research, an Energy Innovation Hub funded by the US Department of Energy, Office of Science, Basic Energy Sciences. This research used resources of the Advanced Photon Source, a US Department of Energy (DOE) Office of Science User Facility operated for the DOE Office of Science by Argonne National Laboratory under contract no. DE-AC02-06CH11357. The SAXS experiments were completed at the Stanford Synchrotron Radiation Light Source, a user facility at SLAC National Accelerator Laboratory, and were supported by the US Department of Energy, Office of Science, Office of Basic Energy Sciences under contract no. DE-AC02-76SF00515. H.G.S. acknowledges funding from the German Federal Ministry of Education and Research (BMBF) via Project 05K22PP2. N.P.B. acknowledges numerous insightful discussions with John Newman.

AUTHOR CONTRIBUTIONS

Conceptualization, M.D.G., H.-G.S., C.J.T., and N.P.B.; methodology, M.D.G., H.-G.S., C.J.T., A.M., L.S.G., S.N., and E.M.D; validation, M.D.G, H.-G.S., C.J.T., A.M., and L.S.G.; formal analysis, M.D.G., H.-G.S., C.J.T., A.M., and L.S.G.; investigation, M.D.G., H.-G.S., C.J.T., A.M., L.S.G., C.C., S.N., E.M.D., and Q.Z.; data curation, M.D.G., H.-G.S., A.M., and L.S.G.; writing – original draft, M.D.G. and N.P.B; writing – reviewing & editing; M.D.G., H.-G.S., C.J.T., A.M., L.S.G., M.F.T., and N.P.B, supervision, H.-G.S.,V.S., M.F.T., and N.P.B., funding acquisition, V.S., M.F.T., and N.P.B.

DECLARATION OF INTERESTS

The authors declare no competing financial interest.

Received: July 28, 2023
Revised: October 14, 2023
Accepted: December 11, 2023
Published: January 10, 2024

REFERENCES

1. Newman, J., and Balsara, N.P. (2021). Electrochemical Systems, 4th ed. (Wiley).
2. Villaluenga, I., Pesko, D.M., Timachova, K., Feng, Z., Newman, J., Srinivasan, V., and Balsara, N.P. (2018). Negative Stefan-Maxwell Diffusion Coefficients and Complete Electrochemical Transport Characterization of Homopolymer and Block Copolymer Electrolytes. J. Electrochem. Soc. *165*, A2766–A2773.
3. Choo, Y., Halat, D.M., Villaluenga, I., Timachova, K., and Balsara, N.P. (2020). Diffusion and Migration in Polymer Electrolytes. Prog. Polym. Sci. *103*, 101220.
4. Loo, W.S., Galluzzo, M.D., Li, X., Maslyn, J.A., Oh, H.J., Mongcopa, K.I., Zhu, C., Wang, A.A., Wang, X., Garetz, B.A., and Balsara, N.P. (2018). Phase Behavior of Mixtures of Block Copolymers and a Lithium Salt. J. Phys. Chem. B *122*, 8065–8074.
5. Teran, A.A., and Balsara, N.P. (2014). Thermodynamics of Block Copolymers with and without Salt. J. Phys. Chem. B *118*, 4–17.
6. Grundy, L.S., Galluzzo, M.D., Loo, W.S., Fong, A.Y., Balsara, N.P., and Takacs, C.J. (2022). Inaccessible Polarization-Induced Phase Transitions in a Block Copolymer Electrolyte: An Unconventional Mechanism for the Limiting Current. Macromolecules *55*, 7637–7649.
7. Galluzzo, M.D., Grundy, L.S., Takacs, C.J., Cao, C., Steinrück, H.G., Fu, S., Rivas Valadez, M.A., Toney, M.F., and Balsara, N.P. (2021). Orientation-Dependent Distortion of Lamellae in a Block Copolymer Electrolyte under DC Polarization. Macromolecules *54*, 7808–7821.
8. Mullin, S.A., Stone, G.M., Teran, A.A., Hallinan, D.T., Hexemer, A., and Balsara, N.P. (2012). Current-Induced Formation of Gradient Crystals in Block Copolymer Electrolytes. Nano Lett. *12*, 464–468.
9. Galluzzo, M.D., Loo, W.S., Schaible, E., Zhu, C., and Balsara, N.P. (2020). Dynamic Structure and Phase Behavior of a Block Copolymer Electrolyte under Dc Polarization. ACS Appl. Mater. Interfaces *12*, 57421–57430.
10. Mistry, A., and Srinivasan, V. (2021). Do We Need an Accurate Understanding of Transport in Electrolytes? Joule *5*, 2773–2776.
11. Wang, A.A., Greenbank, S., Li, G., Howey, D.A., and Monroe, C.W. (2022). Current-Driven Solvent Segregation in Lithium-Ion Electrolytes. Cell Rep. Phys. Sci. *3*, 101047.
12. Wang, A.A., Gunnarsdóttir, A.B., Fawdon, J., Pasta, M., Grey, C.P., and Monroe, C.W. (2021). Potentiometric MRI of a Superconcentrated Lithium Electrolyte: Testing the Irreversible Thermodynamics Approach. ACS Energy Lett. *6*, 3086–3095.
13. Jung, T., Wang, A.A., and Monroe, C.W. (2023). Overpotential from Cosolvent Imbalance in Battery Electrolytes: LiPF6 in EMC:EC. ACS Omega *8*, 21133–21144.
14. Weber, A.Z., and Newman, J. (2004). Transport in Polymer-Electrolyte Membranes : II. J. Electrochem. Soc. *151*, A311.
15. Mistry, A., and Mukherjee, P.P. (2020). Molar Volume Mismatch: A Malefactor for Irregular Metallic Electrodeposition with Solid Electrolytes. J. Electrochem. Soc. *167*, 082510.
16. Wang, J., Yan, Y., Liu, H., Zhang, G., Yue, D., Tong, S., Gao, C., and Han, Y. (2020). Pressure-Induced Ionic to Mixed Ionic and Electronic Conduction Transition in Solid Electrolyte LaF3. Phys. Chem. Chem. Phys. *22*, 26306–26311.
17. Schichtel, N., Korte, C., Hesse, D., and Janek, J. (2009). Elastic Strain at Interfaces and Its Influence on Ionic Conductivity in Nanoscaled Solid Electrolyte Thin Films—Theoretical Considerations and Experimental Studies. Phys. Chem. Chem. Phys. *11*, 3043–3048.
18. Yamakov, V.I., Rains, A.A., Kang, J.H., Das, L., Rashid, R., Su, J., Viggiano, R.P., Connell, J.W., and Lin, Y. (2023). Pressure Dependence of Solid Electrolyte Ionic Conductivity: A Particle Dynamics Study. ACS Appl. Mater. Interfaces *15*, 27243–27252.
19. Jagad, H.D., Harris, S.J., Sheldon, B.W., and Qi, Y. (2022). Tradeoff between the Ion Exchange-Induced Residual Stress and Ion Transport in Solid Electrolytes. Chem. Mater. *34*, 8694–8704.
20. Kusoglu, A., and Weber, A.Z. (2015). Electrochemical/Mechanical Coupling in Ion-Conducting Soft Matter. J. Phys. Chem. Lett. *6*, 4547–4552.
21. Shen, K.-H., Brown, J.R., and Hall, L.M. (2018). Diffusion in Lamellae, Cylinders, and Double Gyroid Block Copolymer Nanostructures. ACS Macro Lett. *7*, 1092–1098.
22. Shen, K.-H., and Hall, L.M. (2020). Ion Conductivity and Correlations in Model Salt-Doped Polymers: Effects of Interaction Strength and Concentration. Macromolecules *53*, 3655–3668.
23. Nakamura, I., and Wang, Z.G. (2012). Salt-Doped Block Copolymers: Ion Distribution, Domain Spacing and Effective χParameter. Soft Matter *8*, 9356–9367.
24. Kambe, Y., Arges, C.G., Czaplewski, D.A., Dolejsi, M., Krishnan, S., Stoykovich, M.P., De Pablo, J.J., and Nealey, P.F. (2019). Role of Defects in Ion Transport in Block Copolymer Electrolytes. Nano Lett. *19*, 4684–4691.
25. Zhang, Z., Krajniak, J., and Ganesan, V.A. (2021). Multiscale Simulation Study of Influence of Morphology on Ion Transport in Block Copolymeric Ionic Liquids. Macromolecules *54*, 5010.
26. Son, C.Y., and Wang, Z.G. (2020). Ion Transport in Small-Molecule and Polymer Electrolytes. J. Chem. Phys. *153*, 100903.
27. Maslyn, J.A., Frenck, L., Veeraraghavan, V.D., Müller, A., Ho, A.S., Marwaha, N., Loo, W.S., Parkinson, D.Y., Minor, A.M., and Balsara, N.P. (2021). Limiting Current in Nanostructured Block Copolymer Electrolytes. Macromolecules *54*, 4010–4022.
28. Kim, O., Jo, G., Park, Y.J., Kim, S., and Park, M.J. (2013). Ion Transport Properties of Self-Assembled Polymer Electrolytes: The Role of Confinement and Interface. J. Phys. Chem. Lett. *4*, 2111–2117.
29. Mistry, A., Srinivasan, V., and Steinrück, H. (2023). Characterizing Ion Transport in Electrolytes via Concentration and Velocity Profiles. Adv. Energy Mater. *13*, 2203690.
30. Halat, D.M., Mistry, A., Hickson, D., Srinivasan, V., Balsara, N.P., and Reimer, J.A. (2023). Transference Number of Electrolytes from the Velocity of a Single Species Measured by Electrophoretic NMR. J. Electrochem. Soc. *170*, 030535.
31. Lorenz, M., Kilchert, F., Nürnberg, P., Schammer, M., Latz, A., Horstmann, B., and Schönhoff, M. (2022). Local Volume Conservation in Concentrated Electrolytes Is Governing Charge Transport in Electric Fields. J. Phys. Chem. Lett. *13*, 8761–8767.
32. Steinrück, H.G., Takacs, C.J., Kim, H.-K., Mackanic, D.G., Holladay, B., Cao, C., Narayanan, S., Dufresne, E.M., Chushkin, Y., Ruta, B., et al. (2020). Concentration and Velocity Profiles in a Polymeric Lithium-Ion Battery Electrolyte. Energy Environ. Sci. *13*, 4312–4321.
33. Steinrück, H.G. (2021). General Relationship between Salt Concentration and X-Ray Absorption for Binary Electrolytes. AIP Adv. *11*, 115119.
34. Galluzzo, M.D., Loo, W.S., Wang, A.A., Walton, A., Maslyn, J.A., and Balsara, N.P. (2020). Measurement of Three Transport Coefficients and the Thermodynamic Factor in Block Copolymer Electrolytes with Different Morphologies. J. Phys. Chem. B *124*, 921–935.
35. Berne, B.J., and Pecora, R. (1976). Dynamic Light Scattering with Applications to Chemistry, Biology, and Physics (Courier Corporation)).
36. Livet, F., Bley, F., Ehrburger-Dolle, F., Morfin, I., Geissler, E., and Sutton, M. (2006). X-Ray Intensity Fluctuation Spectroscopy by Heterodyne Detection. J. Synchrotron Radiat. *13*, 453–458.
37. Ehrburger-Dolle, F., Morfin, I., Bley, F., Livet, F., Heinrich, G., Richter, S., Piché, L., and Sutton, M. (2012). XPCS Investigation of the Dynamics of Filler Particles in Stretched Filled Elastomers. Macromolecules *45*, 8691–8701.
38. Ulbrandt, J.G., Rainville, M.G., Wagenbach, C., Narayanan, S., Sandy, A.R., Zhou, H., Ludwig Jr, K.F., and Headrick, R.L. (2016). Direct Measurement of the Propagation Velocity of Defects Using Coherent X-Rays. Nat. Phys. *12*, 794–799.
39. Lhermitte, J.R.M., Rogers, M.C., Manet, S., and Sutton, M. (2017). Velocity Measurement by Coherent X-Ray Heterodyning. Rev. Sci. Instrum. *88*, 015112.
40. Fredrickson, G.H., and Helfand, E. (1987). Fluctuation Effects in the Theory of Microphase Separation in Block Copolymers. J. Chem. Phys. *87*, 697–705.
41. Leibler, L. (1980). Theory of Microphase Separation in Block Copolymers. Macromolecules *13*, 1602–1617.
42. Gomez, E.D., Panday, A., Feng, E.H., Chen, V., Stone, G.M., Minor, A.M., Kisielowski, C., Downing, K.H., Borodin, O., Smith, G.D., and Balsara, N.P. (2009). Effect of Ion Distribution

on Conductivity of Block Copolymer Electrolytes. Nano Lett. *9*, 1212–1216.

43. Mistry, A., Grundy, L.S., Halat, D.M., Newman, J., Balsara, N.P., and Srinivasan, V. (2022). Effect of Solvent Motion on Ion Transport in Electrolytes. J. Electrochem. Soc. *169*, 040524.

44. Pesko, D.M., Timachova, K., Bhattacharya, R., Smith, M.C., Villaluenga, I., Newman, J., and Balsara, N.P. (2017). Negative Transference Numbers in Poly(Ethylene Oxide)-Based Electrolytes. J. Electrochem. Soc. *164*, E3569–E3575.

45. Ma, Y., Doyle, M., Fuller, T.F., Doeff, M.M., De Jonghe, L.C., and Newman, J. (1995). The Measurement of a Complete Set of Transport Properties for a Concentrated Solid Polymer Electrolyte Solution. J. Electrochem. Soc. *142*, 1859–1868.

46. Evans, J., Vincent, C.A., and Bruce, P.G. (1987). Electrochemical Measurement of Transference Numbers in Polymer Electrolytes. Polymer *28*, 2324–2328.

47. Mistry, A., Verma, A., Sripad, S., Ciez, R., Sulzer, V., Brosa Planella, F., Timms, R., Zhang, Y., Kurchin, R., Dechent, P., et al. (2021). Minimal Information Set to Enable Verifiable Theoretical Battery Reseach. ACS Energy Lett. *6*, 3831–3835.